Supplementary information

Reprogramming mitochondrial metabolism and epigenetics of macrophages via miR-10a liposomes for atherosclerosis therapy

Fei Fang[1], Erxiang Wang[1], Hanqiao Yang[1], Ting Zhao[1], Qiwei Wang[1], Zhen Zhang[2], Yang Song[1], Xiaoheng Liu[1]*

1. Institute of Biomedical Engineering, West China School of Basic Medical Sciences & Forensic Medicine, Sichuan University, Chengdu 610041, China.

2. Department of Cardiology, the Third People's Hospital of Chengdu, Affiliated Hospital of Southwest Jiaotong University, Chengdu 610000, China.

* Corresponding author: *Xiaoheng Liu: liuxiaohg@scu.edu.cn;*

Inventory of Supporting Information

Table S1. The sequences miR-10a-5p and miRNC

Name	Sequences (5'→3')
miR-10a-5p	UACCCUGUAGAUCCGAAUUUGUG
miRNC	UUGUACUACACAAAAGUACUG

Table S2. Primer sequence for qRT-PCR

Gene	Primer sequences (5'→3')
Sirt1 (Mouse)	F: TGATTGGCACCGATCCTCG
	R: CCACAGCGTCATATCATCCAG
Ppargc1b (Mouse)	F: CTTGGCTGCGCTTACGAAGA
	R: GAAAGCTCGTCCACGTCAGAC
Acox1 (Mouse)	F: TAACTTCCTCACTCGAAGCCA
	R: AGTTCCATGACCCATCTCTGTC
Acox3 (Mouse)	F: ACCGGAAGAAAAAGACAGTGC
	R: GAGGCTCTTGCTCGGTAGG
Idh3a (Mouse)	F: TGGGTGTCCAAGGTCTCTC
	R: CTCCCACTGAATAGGTGCTTTG
Ogdh (Mouse)	F: GTTTCTTCAAACGTGGGGTTCT
	R: GCATGATTCCAGGGGTCTCAAA
IL-1β (Mouse)	F: GAAATGCCACCTTTTGACAGTG
	R: TGGATGCTCTCATCAGGACAG
TNF-α (Mouse)	F: GGCAGGTTCTGTCCCTTT
	R: TGCTTTCTGTGCTCATGGT

NOS2 (Mouse)	F: GTTCTCAGCCCAACAATACAAGA
	R: GTGGACGGGTCGATGTCAC
Arg1 (Mouse)	F: CTCCAAGCCAAAGTCCTTAGAG
	R: GGAGCTGTCATTAGGGACATCA
Mrc1 (Mouse)	F: CTCTGTTCAGCTATTGGACGC
	R: TGGCACTCCCAAACATAATTTGA

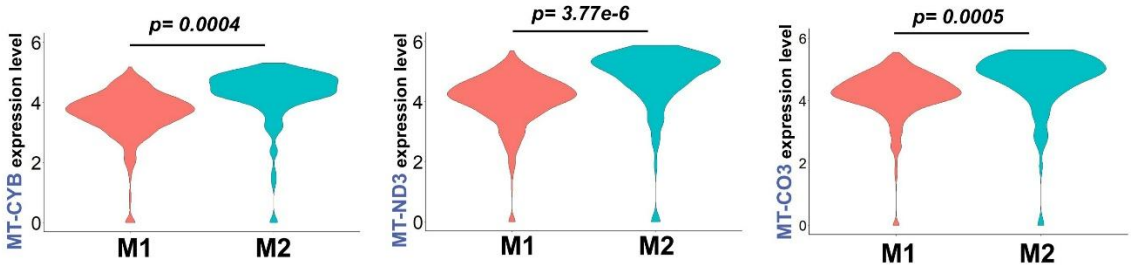

Figure S1. Expression of mitochondrial function-related genes in M1 and M2 phenotype populations.

Violin plots show the differential expression of MT-CYB, MT-ND3, and MT-CO3 in each cluster of M1 phenotype and M2 phenotype macrophages in the human atherosclerotic plaque. Data analyzed by two-tailed Wilcoxon rank-sum test (Mann-Whitney U test).

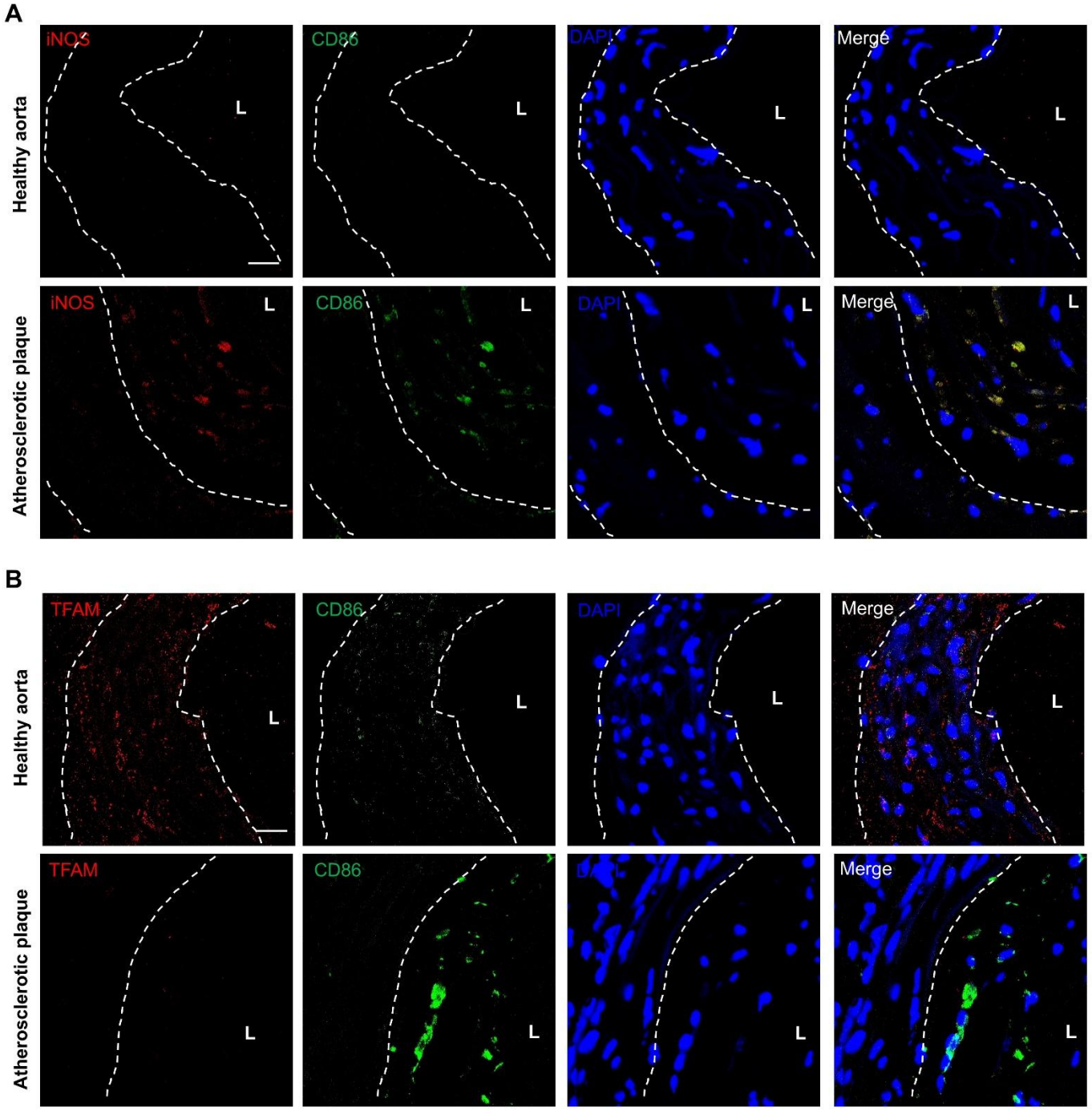

Figure S2. Evaluation of mitochondrial function of macrophages in aorta of atherosclerotic mice by immunofluorescence staining.

Immunofluorescence imaging of M1 phenotype macrophage ($CD86^+$)/iNOS and M1 phenotype macrophage ($CD86^+$)/TFAM in the healthy and atherosclerotic mice aorta samples, scale bar: 20 μm. The vascular lumen is denoted by L.

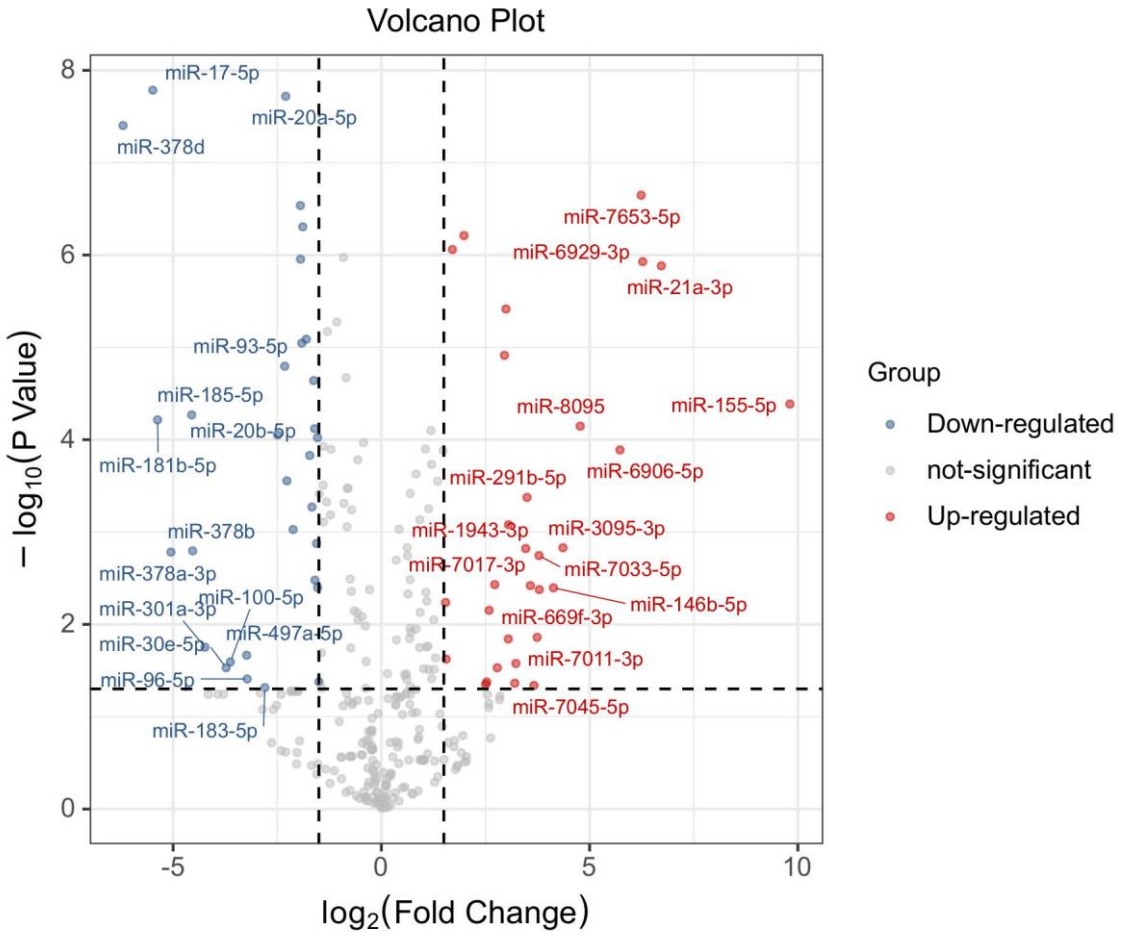

Figure S3. Volcano plot of differentially expressed miRNAs between M1-type macrophages and M0-type macrophages.

The volcano plot shows the 30 upregulated and 31 downregulated miRNAs between the inflammation macrophage and control group.

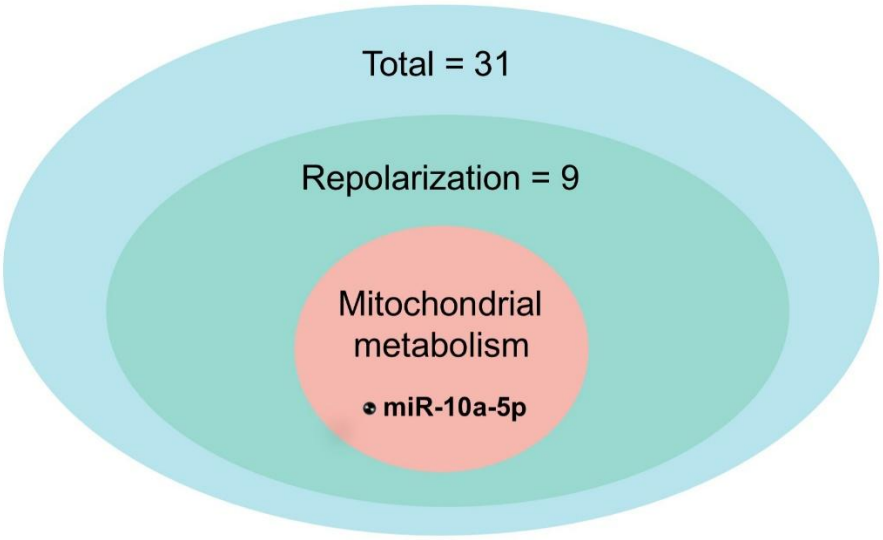

Figure S4. Venn diagram of upregulated miRNAs in M1 macrophages associated with macrophage phenotype and mitochondrial functional reprogramming.

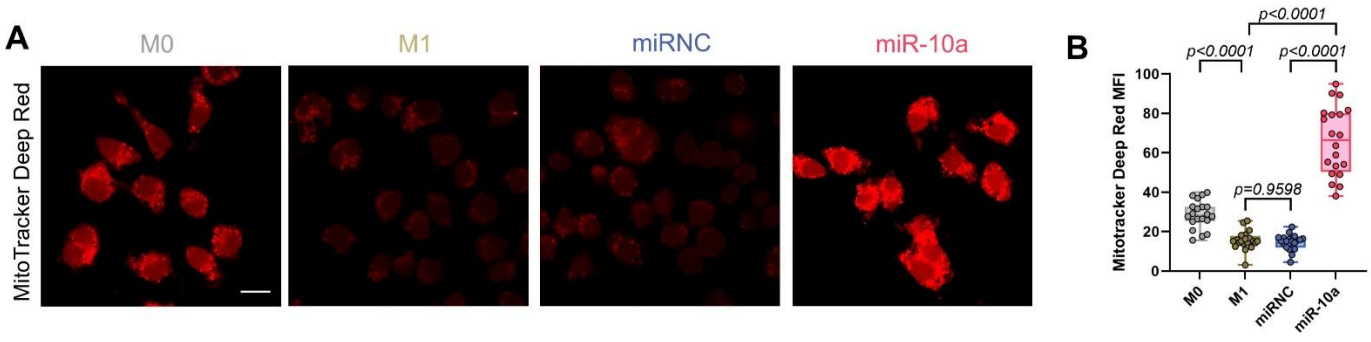

Figure S5. Evaluation of the effect of miR-10a on mitochondrial function of M1 phenotype macrophages by Mitotrack deep red staining.

(A) CLSM image and mean fluorescence intensity (B) of Mitoracker deep red staining after miR-10a transfected, scale bar: 20 μm. Data in panel (B) are shown as the mean ± SD (n=20 fields from 5 independent samples, One-way ANOVA analysis followed by Tukey's multiple comparisons test).

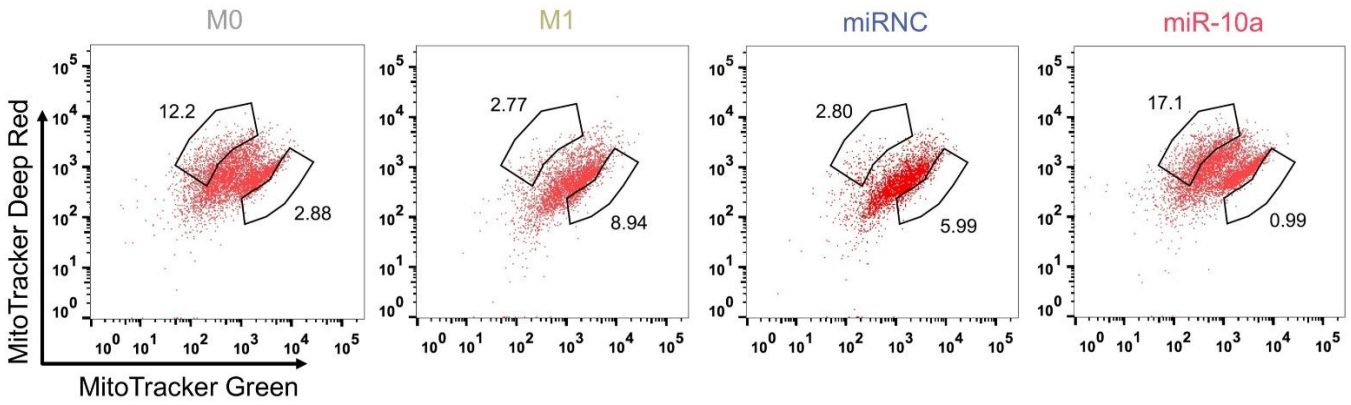

Figure S6. Evaluation of the effect of miR-10a on mitochondrial function of M1 phenotype macrophages by flow cytometry.

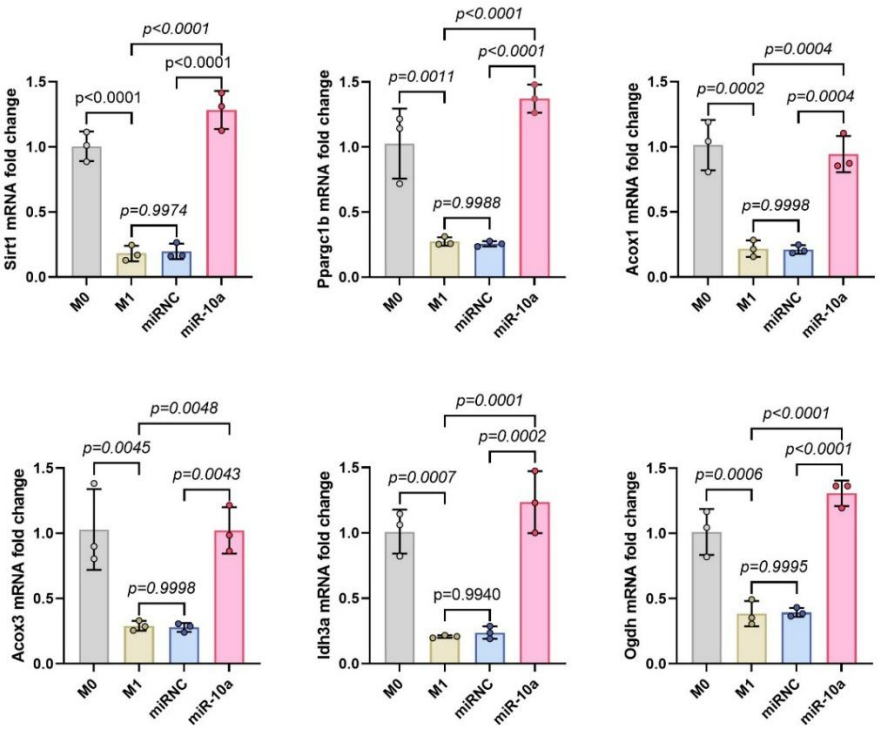

Figure S7. qRT-PCR evaluation of the effect of miR-10a on mitochondrial function of M1 phenotype macrophages.

qRT-PCR analysis of the expression of mitochondrial biogenesis-related genes *Sirt1*, *Ppargc1b*, FAO-related genes *Acox1*, *Acox3*, and OXPHOS-related genes *Idh3a*, *Ogdh*. Data are shown as the mean ± SD (n=3 independent samples, One-way ANOVA analysis followed by Tukey's multiple comparisons test).

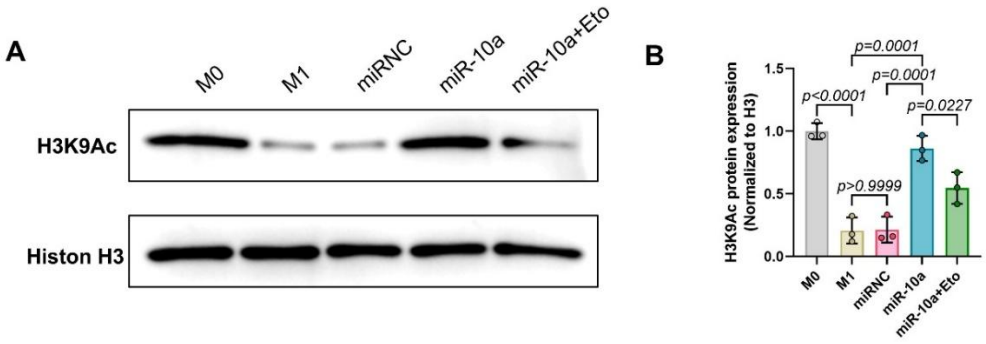

Figure S8. Effects of miR-10a treatment on histone acetylation level in M1 phenotype macrophages.

(A) Histones were extracted from cells in different treatment groups, western blotting analysis of the expression of H3K9Ac, Histon H3 as loading control. (B) The grayscale values of blots were quantified using Image J software. Panel (B) data are presented as the mean ± SD (n=3 independent samples, One-way ANOVA analysis followed by Tukey's multiple comparisons test).

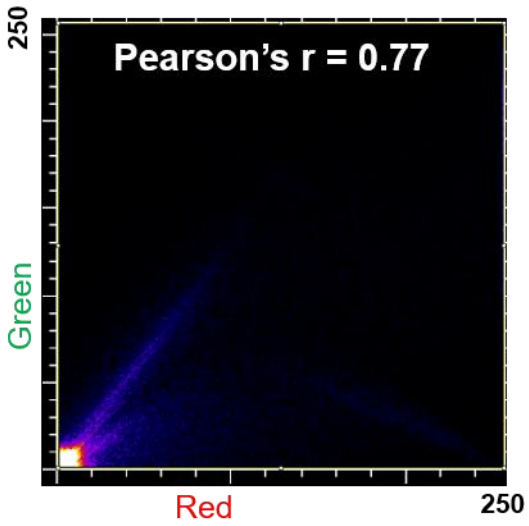

Figure S9. **Pearson's correlation coefficient of fluorescence image (Figure 4e).**

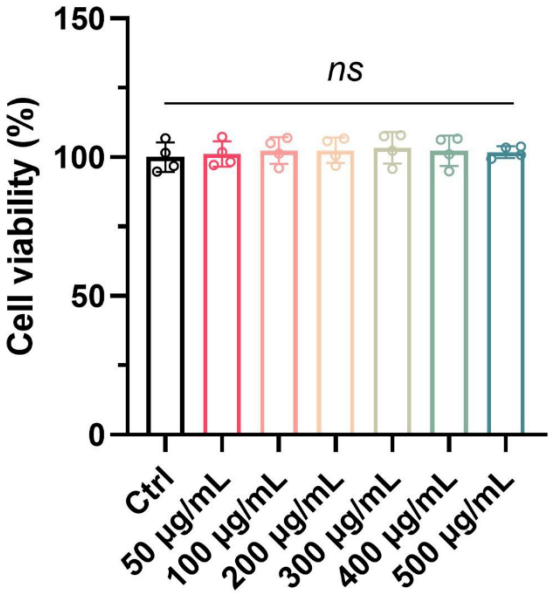

Figure S10. **In vitro cytotoxicity evaluation of H-MNP.**

Data are shown as the mean ± SD (n=4 independent samples, One-way ANOVA analysis followed by Tukey's multiple comparisons test).

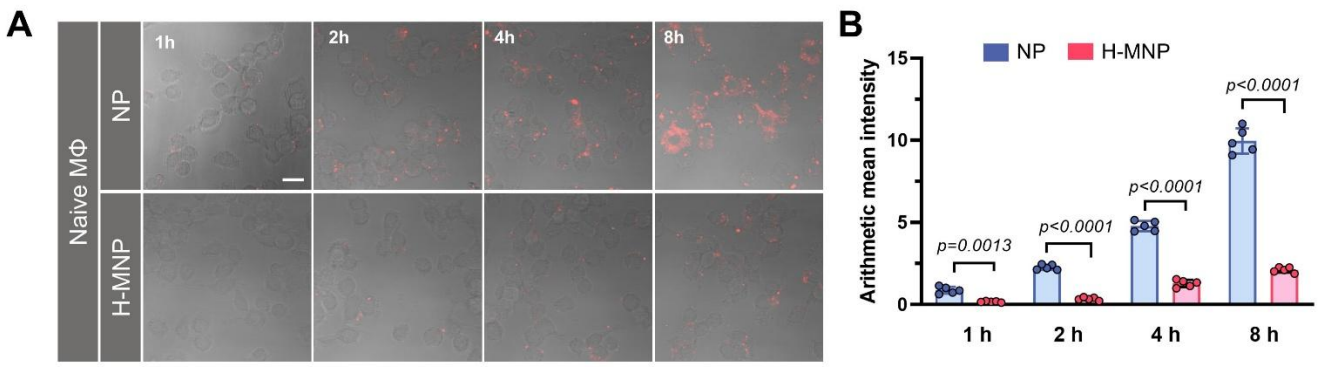

Figure S11. **Cellular uptake of H-MNP by Naïve macrophage.**

(A) CLSM image and arithmetic mean intensity (B) of cy5-miR-10a@H-MNP or cy5-miR-10a@NP incubated with naive macrophage with different times (1, 2, 4, 8 hours), scare bar: 20 μm. Data are shown as the mean ± SD (n=5 independent samples, two-tailed unpaired Student *t* test).

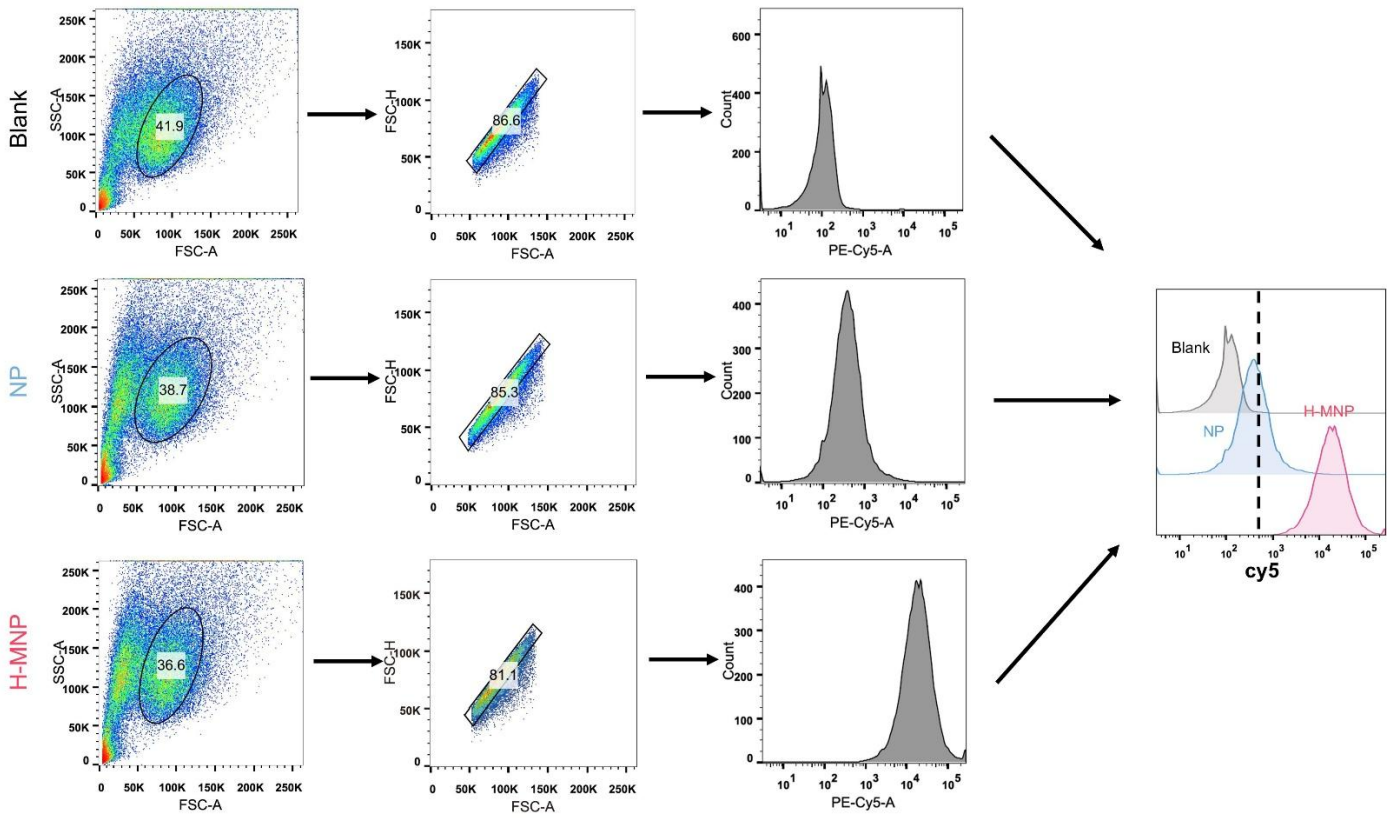

Figure S12. **Flow cytometric plots of NP and H-MNP cellular uptake.**

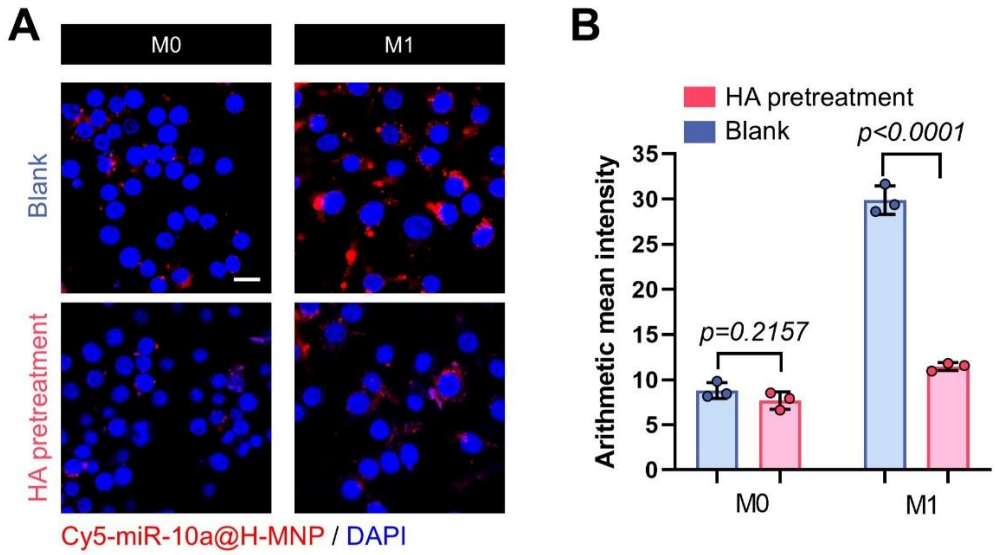

Figure S13. Cellular uptake of H-MNP by M1-phenotype macrophage.

(A) CLSM image and arithmetic mean intensity (B) of H-MNP uptake by M0 and M1 phenotype macrophage with or without HA pretreatment, scale bar: 20 μm. Data in panel (B) are shown as the mean ± SD (n=3 independent samples, two-tailed unpaired student *t* test).

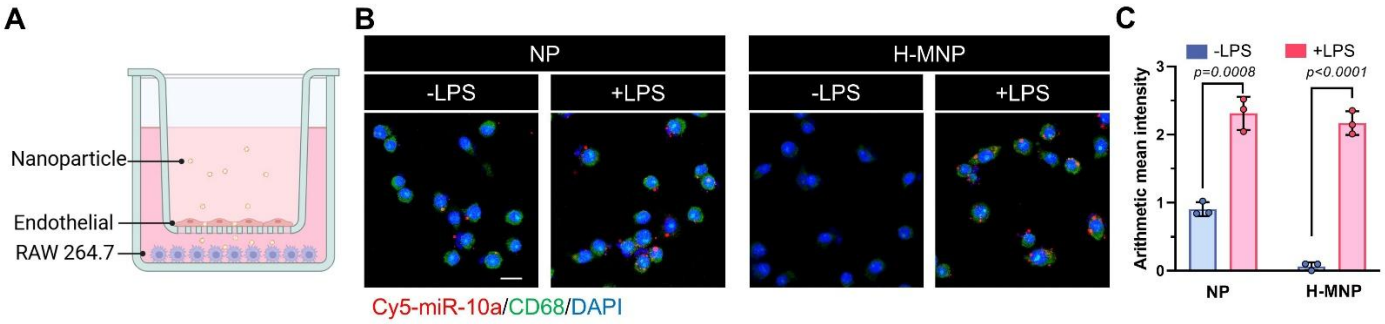

Figure S14. Transwell model to evaluate the internalization of H-MNP by macrophages after trans-endothelial.

(A) Schematic diagram of the Transwell model. HUVECs were seeded in the upper chamber and RAW264.7 cells were seeded in the lower chamber. HUVECs were stimulated with LPS for 24 hours, and cy5-miR-10a@NP and cy5-miR-10a@H-MNP were added to the upper chamber and incubated for 8 hours. (B) CLSM image and arithmetic mean intensity (C) of NP in RAW264.7 cells, scare bar: 20 μm. Data in panel (C) are shown as the mean ± SD (n=3 independent samples, two-tailed unpaired student *t* test). Panel **(a)** was created in BioRender. Fang, F. (2025) https://BioRender.com/2wex2f7.

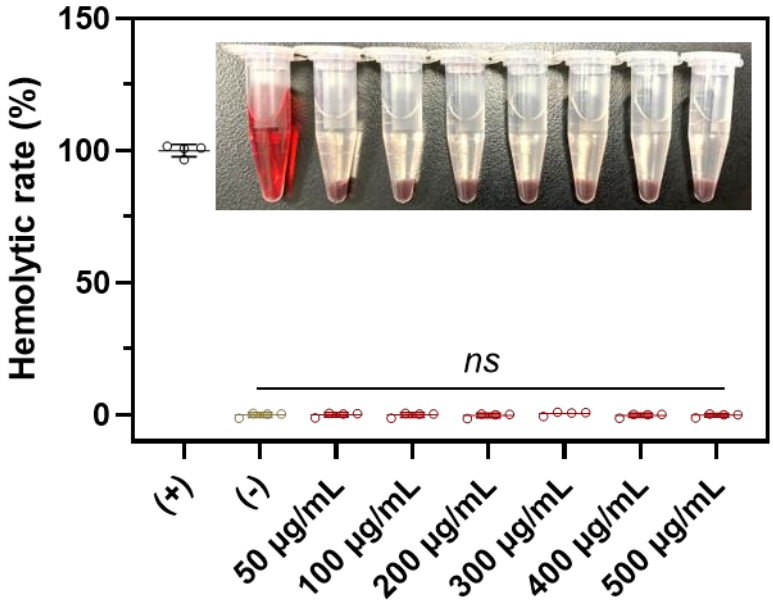

Figure S15. **In vitro hemolytic rate determination of miR-10a@H-MNP.**

Data are shown as the mean ± SD (n=4 independent samples, One-way ANOVA analysis followed by Tukey's multiple comparisons test).

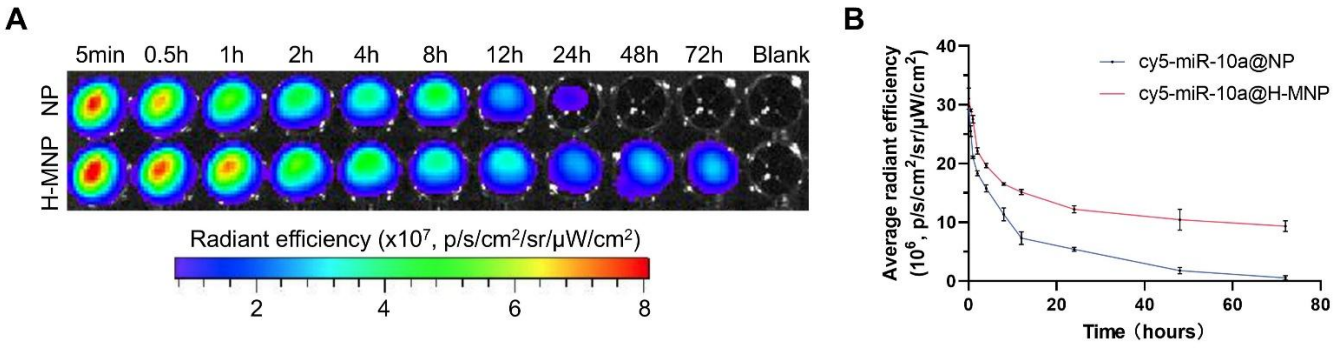

Figure S16. **Evaluation of the circulation duration of H-MNP in mice.**

(A) IVIS images and their quantification (B) of blood at various time intervals following the administration of NP and H-MNP via tail vein injection of 6 hours. Data in panel (B) are shown as the mean ± SD, n=3 independent samples.

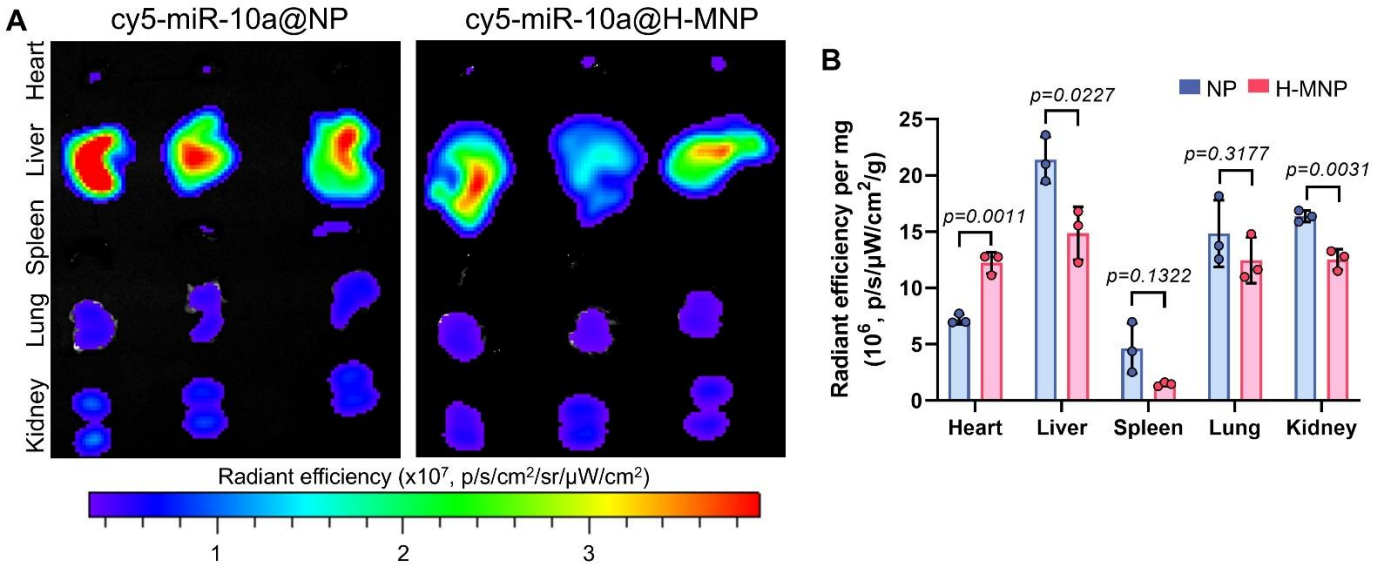

Figure S17. **Distribution of H-MNPs in major organs of mice.**

(A) IVIS image and their quantification (B) of the heart, liver, spleen, lung, and kidney in atherosclerotic mice obtained 6 hours post intravenous administration of NP and H-MNP. Data in panel (B) are shown as the mean ± SD (n=3 independent samples, two-tailed unpaired student *t* test).

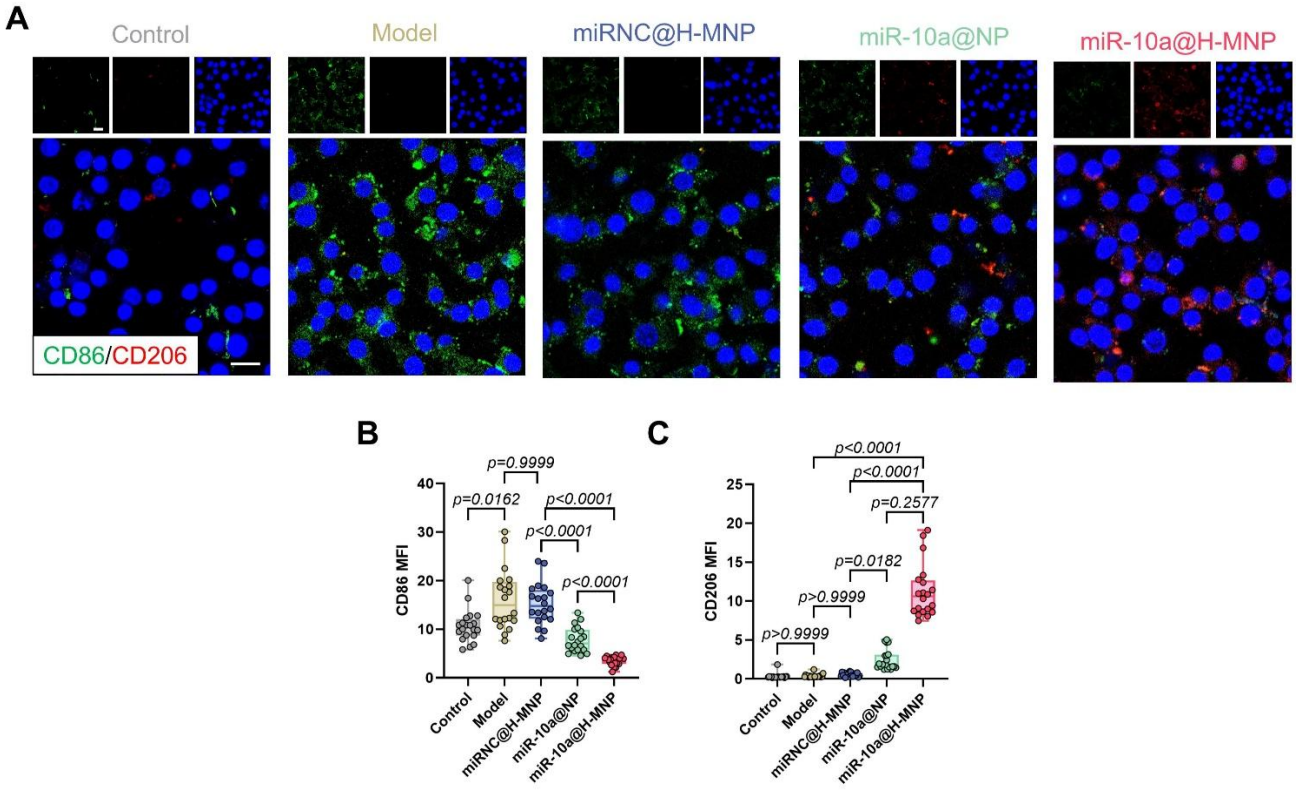

Figure S18. **Effects of miR-10a@H-MNP on phenotypic transformation of macrophages.**

(A) Immunofluorescence image of M1 phenotype macrophage ($CD86^+$) and M2 phenotype macrophage ($CD206^+$) after different treatment and their quantification (B&C), scale bar: 20 μm. Data in panel (B) and (C) are shown as the mean ± SD (n=20 fields from 5 independent samples). P values in (b) were determined by One-way ANOVA analysis followed by Dunnett's T3 multiple comparisons test. P values in (c) were determined by Kruskal-Walli's analysis followed by Dunn's multiple comparison test.

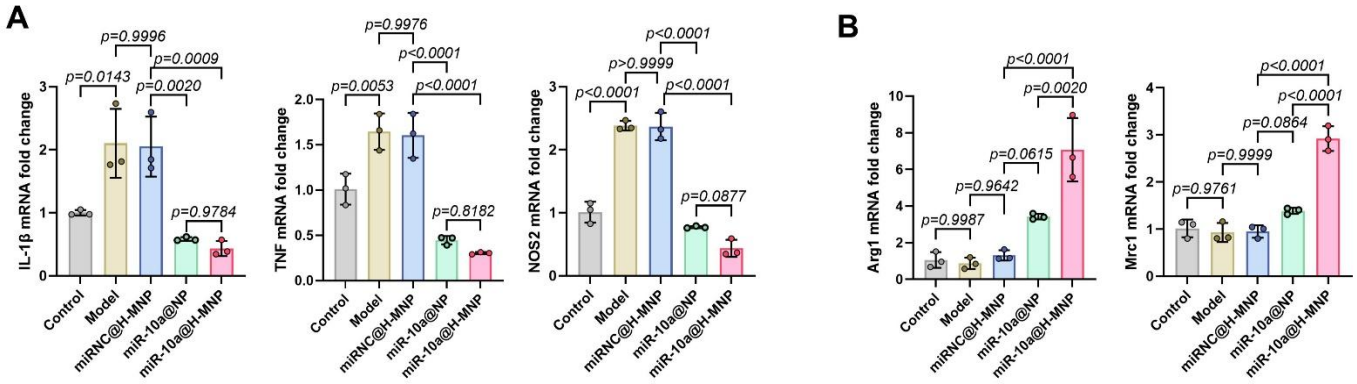

Figure S19. **Effects of miR-10a@H-MNP on phenotypic transformation related genes of macrophages.**

(A) qRT-PCR analysis of the mRNA levels of M1 phenotype relative genes, I*L-1β, TNF-α* and *NOS2*, n = 3. (B) qRT-PCR analysis the mRNA levels of M2 phenotype relative genes, *Arg1* and *Mrc1*. Data are shown as the mean ± SD (n=3 independent samples, One-way ANOVA analysis followed by Tukey's multiple comparisons test).

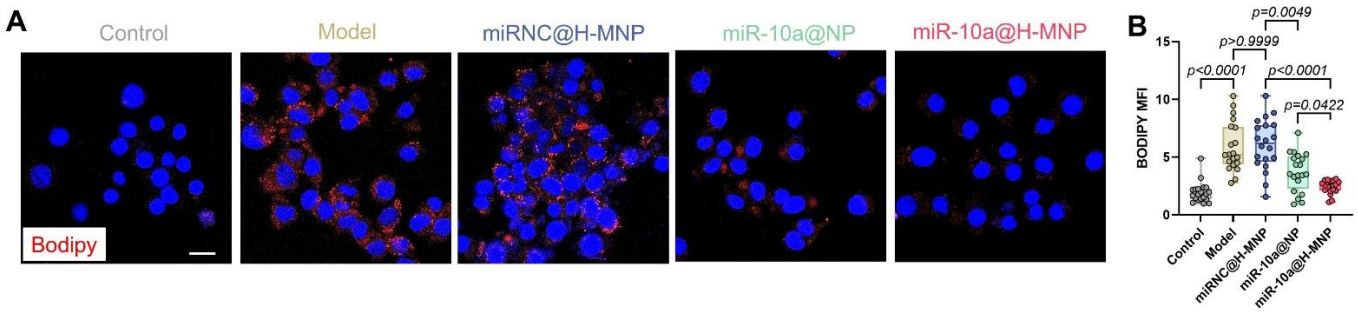

Figure S20. **Effects of miR-10a@H-MNP on lipid uptake of macrophages.**

CLSM image of lipid droplets in macrophage after different treatments and fluorescent intensity quantification analysis, scale bar: 20 μm. Data in panel (B) are shown as the mean ± SD (n=20 fields from 5 independent samples, One-way ANOVA analysis followed by Dunnett's T3 multiple comparisons test).

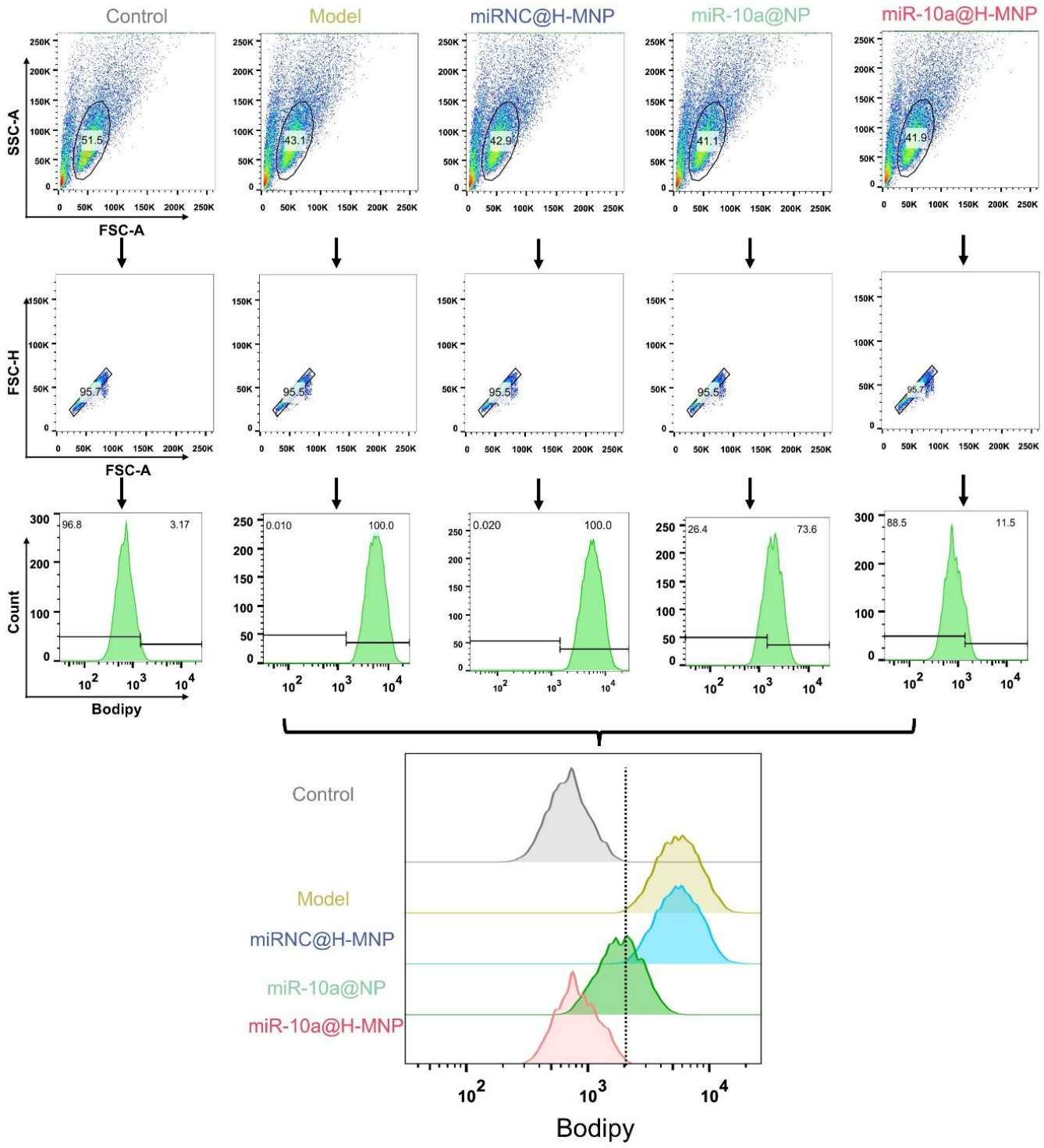

Figure S21. **Flow cytometry analysis of lipid droplet content in macrophages after different treatments.**

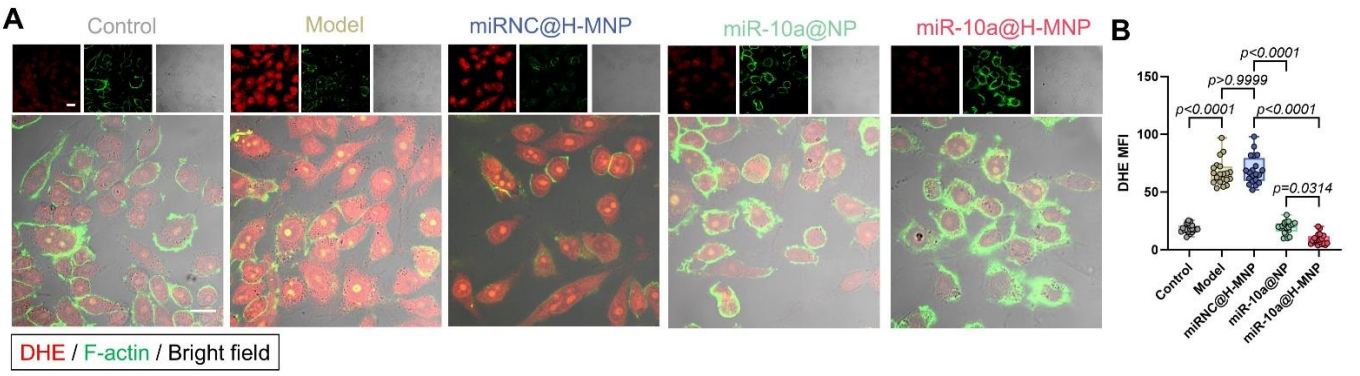

Figure S22. **DHE staining of macrophage after different treatments.**

DHE staining image (A) of macrophage after different treatment and their fluorescence intensity quantification (B), scale bar: 20 μm. Data in panel (B) are shown as the mean ± SD (n=20 fields from 5 independent samples, Kruskal-Walli's analysis followed by Dunn's multiple comparison test).

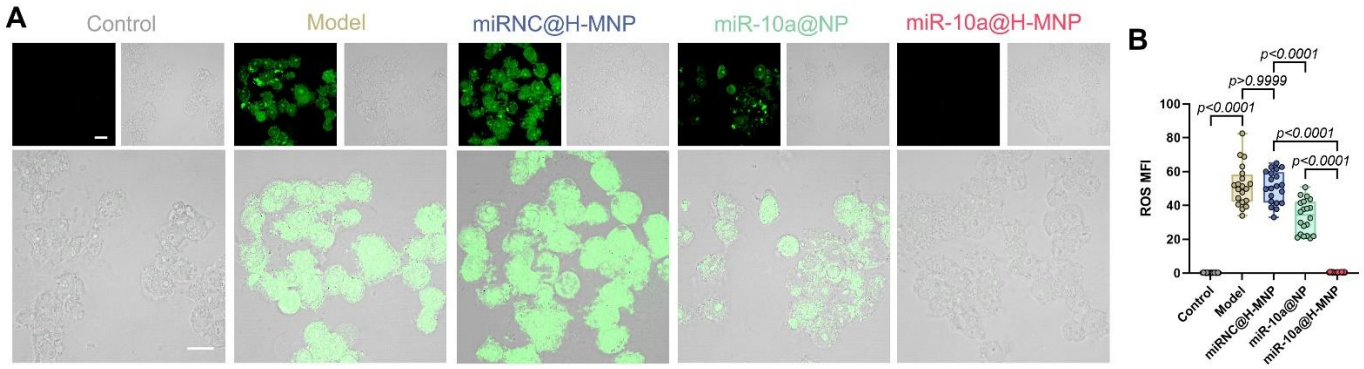

Figure S23. **ROS staining of macrophage after different treatments.**

ROS staining image (A) of macrophage after different treatment and their fluorescence intensity quantification (B), scale bar: 20 μm. Data in panel (B) are shown as the mean ± SD (n=20 fields from 5 independent samples, One-way ANOVA analysis followed by Dunnett's T3 multiple comparisons test).

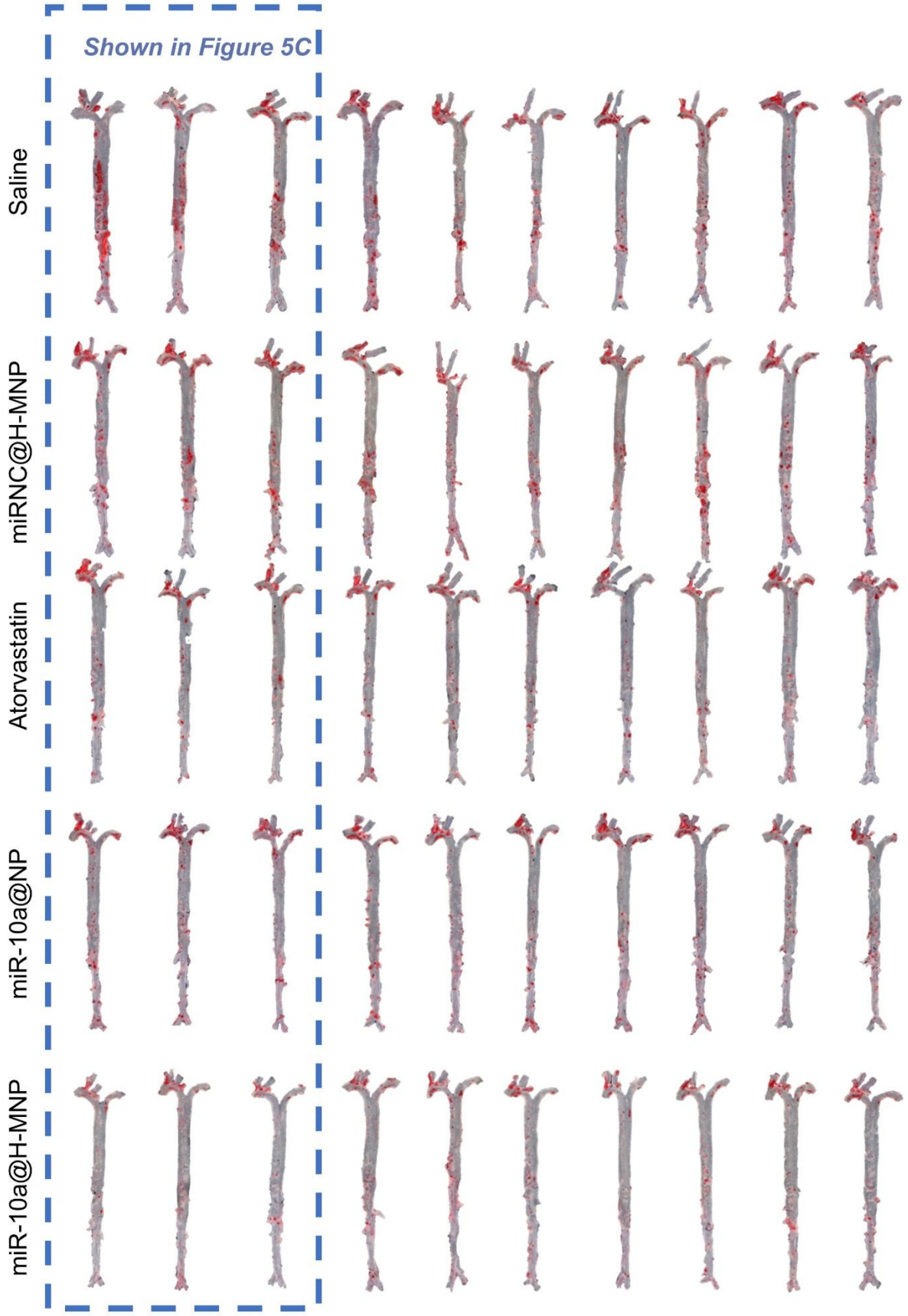

Figure S24. ***En face*** **ORO staining of ApoE$^{-/-}$ mouse aorta after treatment with different formulations**.

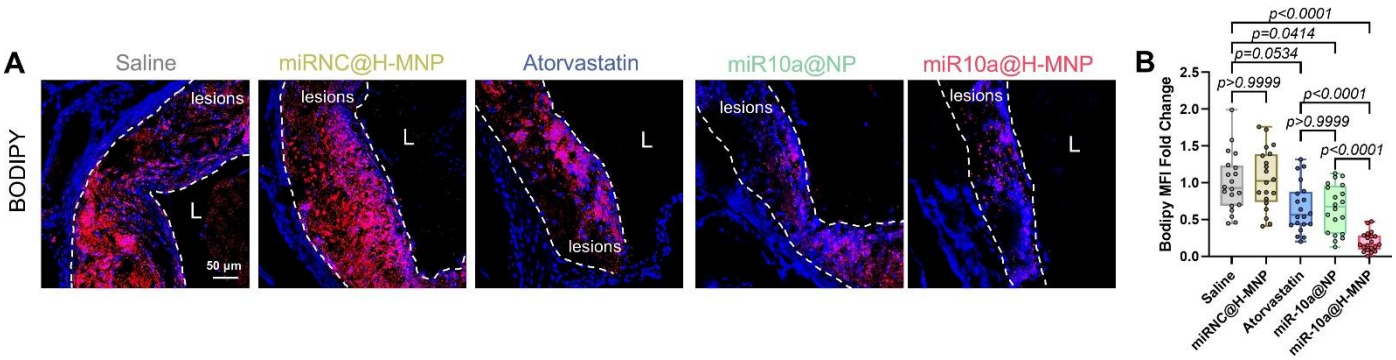

Figure S25. **Bodipy staining of macrophage after different treatments.**

(A) CLSM images and fluorescence intensity quantification (B) of aortic root BODIPY staining. Data in panel (B) are shown as the mean ± SD (n=20 sections from 5 independent samples, One-way ANOVA analysis followed by Dunnett's T3 multiple comparisons test).

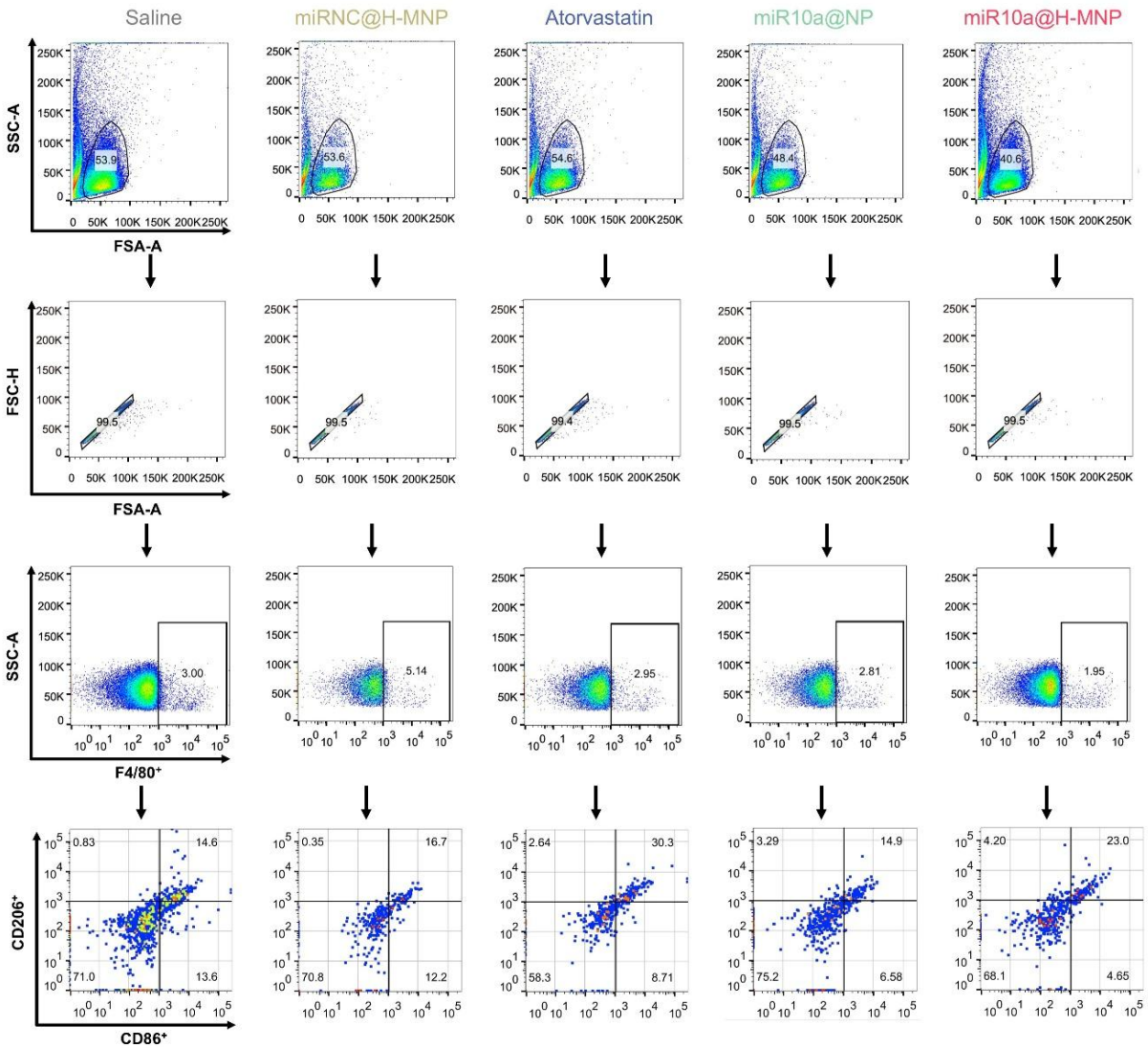

Figure S26. Flow cytometric plots of phenotype change of macrophage in the aorta after different treatments.

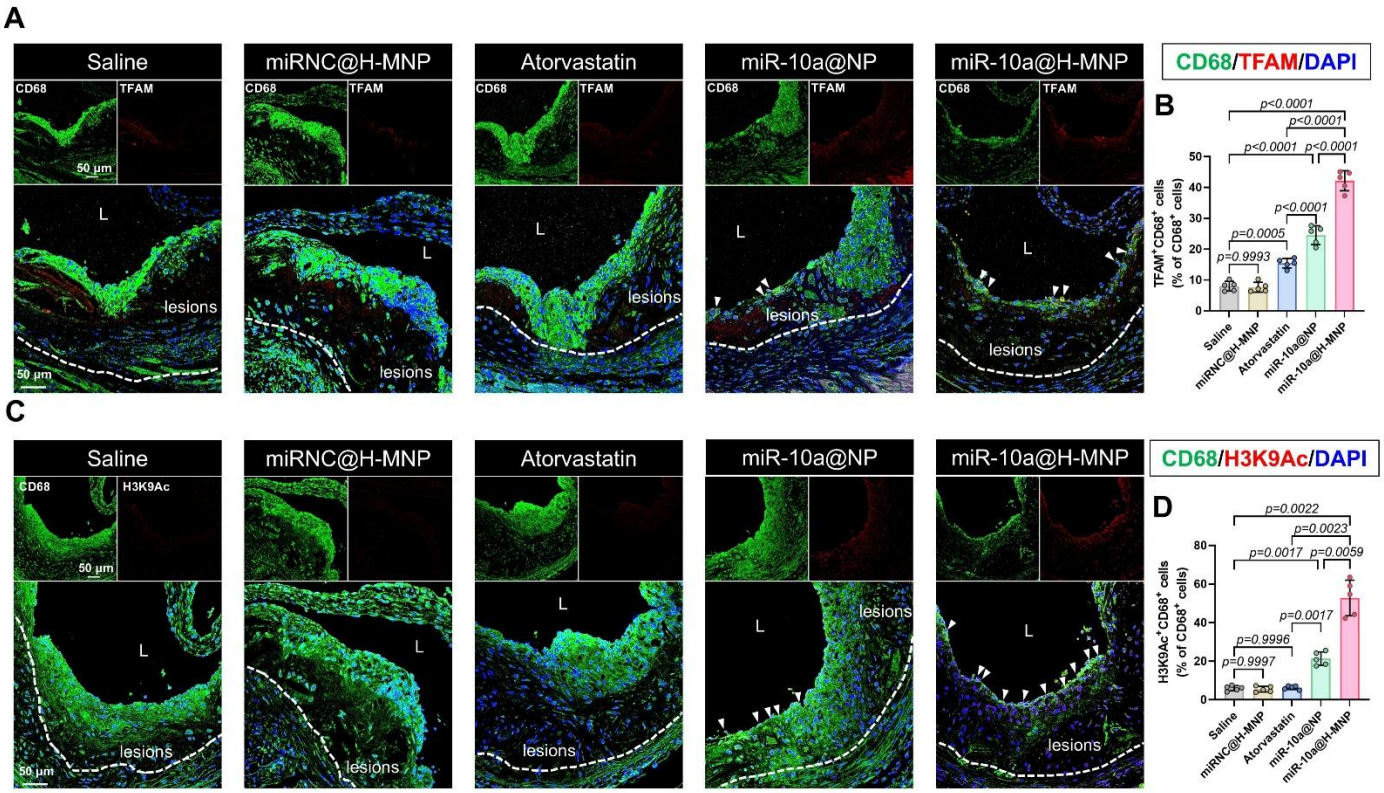

Figure S27. **The mitochondrial function and histone acetylation level of mouse aortic roots macrophages after different treatments.**

(A) Immunofluorescence staining of aortic root for CD68 and TFAM and quantification of the TFAM and CD68 positive cells number by image J (B). (C) Immunofluorescence staining of aortic root for CD68 and H3K9Ac and quantification of the H3K9Ac and CD68 positive cells number by image J (D). Data in panel (B&D) are shown as the mean ± SD (n= 5 independent samples). P values in (b) were determined by One-way ANOVA analysis followed by Tukey's multiple comparisons test. P values in (d) were determined by One-way ANOVA analysis followed by Dunnett's T3 multiple comparisons test.

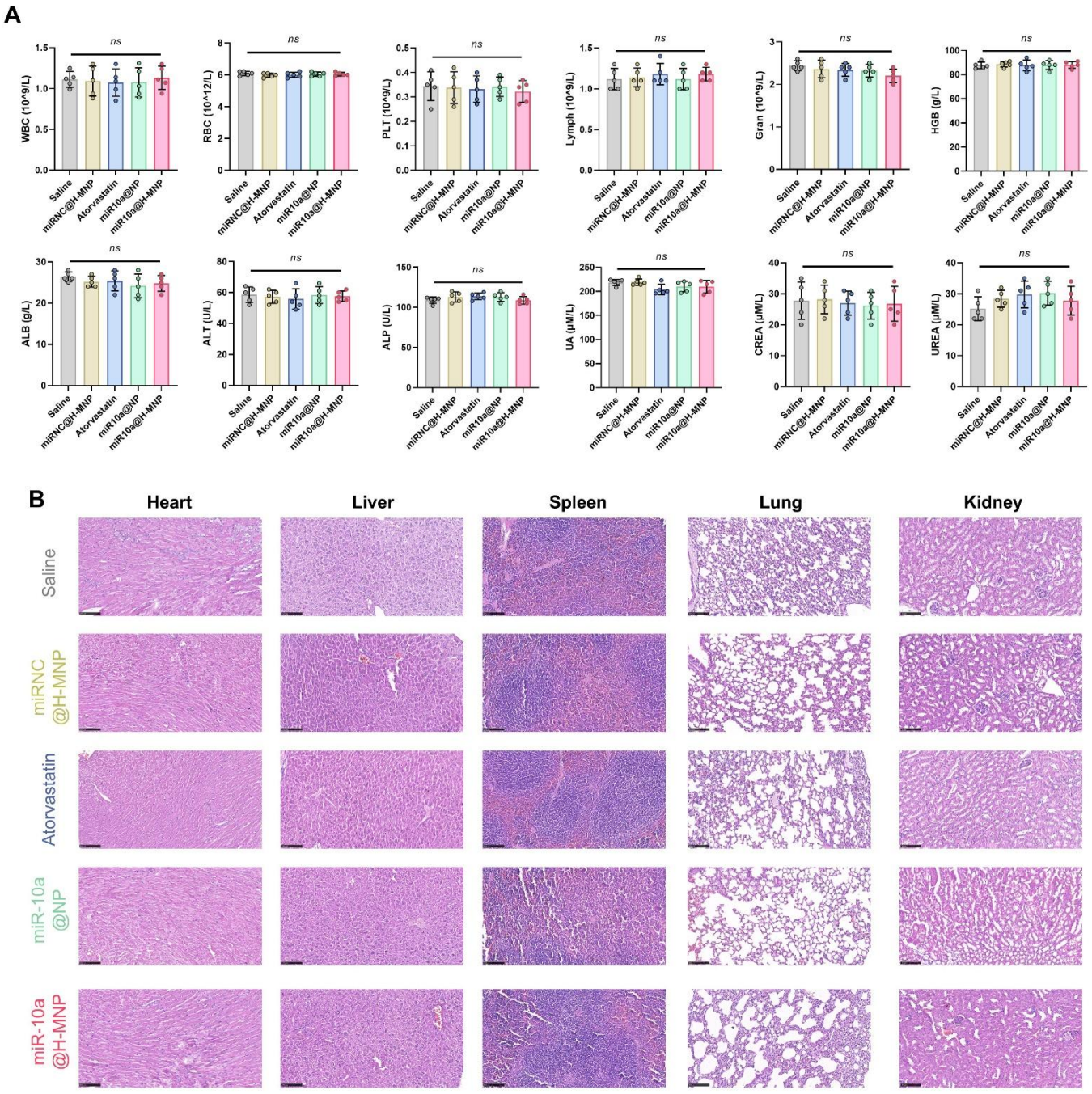

Figure S28. Toxicological evaluations and H&E staining after four weeks of treatment.

(A) Routine blood and biochemical assays. Red blood cells (RBC), white blood cells (WBC), platelets (PLT), lymphocytes, neutrophil granulocytes (GRAN), hemoglobin (HGB), albumin (ALB), aminotransferase (ALT), alkaline phosphatase (ALP), uric acid (UA), creatinine (CREA), UREA. (B) H&E-stained images of main organs from mice (scale bar: 100μm). Data in panel (A) are shown as the mean ± SD (n=5 independent samples, One-way ANOVA analysis followed by Tukey's multiple comparisons test).